Do Biophysical Properties of the Airway Smooth Muscle in Culture Predict Airway Hyperresponsiveness?

Steven S. An, Ben Fabry, Xavier Trepat, Ning Wang, and Jeffrey J. Fredberg

Physiology Program, Department of Environmental Health, Harvard School of Public Health, Boston, Massachusetts; Division of Physiology, Department of Environmental Health Sciences, Johns Hopkins Bloomberg School of Public Health, Baltimore, Maryland; and Department of Physics, Erlangen University, Erlangen, Germany

Airway hyperresponsiveness is a cardinal feature of asthma but remains largely unexplained. In asthma, the key end-effector of acute airway narrowing is the airway smooth muscle (ASM) cell. Here we report novel biophysical properties of the ASM cell isolated from the relatively hyporesponsive Lewis rat versus the relatively hyperresponsive Fisher rat. We focused upon the ability of the cytoskeleton (CSK) of the ASM cell to stiffen, to generate contractile forces, and to remodel. We used optical magnetic twisting cytometry to measure cell stiffness and traction microscopy to measure contractile forces. To measure remodeling dynamics, we quantified spontaneous nanoscale motions of a microbead tightly anchored to the CSK. In response to a panel of contractile and relaxing agonists, Fisher ASM cells showed greater stiffening, bigger contractile forces, and faster CSK remodeling; they also exhibited higher effective temperature of the CSK matrix. These physical differences measured at the level of the single cell *in vitro* were consistent with strain-related differences in airway responsiveness *in vivo*. As such, comprehensive biophysical characterizations of CSK dynamics at the level of the cell in culture may provide novel perspectives on the ASM and its contributions to the excessive airway narrowing in asthma.

Keywords: airway hyperresponsiveness; airway smooth muscle; cytoskeleton dynamics; inbred strains; remodeling

Airway hyperresponsiveness (AHR) is the ability of the airways to narrow too easily and too much (1, 2). AHR is a cardinal feature of asthma, but its mechanisms remain largely unexplained. Acute narrowing of the airway lumen is caused by contraction of the airway smooth muscle (ASM) cell (3–5). The ASM cell plays an important role in asthma pathophysiology, including AHR, but evidence for a causal link between AHR and an altered ASM contractility has been at best equivocal (6, 7).

Contraction of the ASM cell is driven by the myosin motor, and myosin exerts its mechanical effects within an integrated cytoskeletal scaffolding. The contractile apparatus and its scaffolding are dynamic structures that are in a continuous state of remodeling (8–11). Moreover, the ASM cell can extensively remodel these internal microstructures to produce a robust muscle force over a wide range of muscle lengths (12–16). It is thought that this ability of the ASM cell to accommodate its cytoskeleton (CSK) to progressively shorter working muscle lengths is a major factor contributing to the excessive airway narrowing in asthma.

(*Received in original form December 10, 2005 and in final form February 13, 2006*)

This work was supported by National Heart, Lung, and Blood Institute grants HL-59682 and HL-33009.

Correspondence and requests for reprints should be addressed to Steven S. An, Ph.D., Johns Hopkins University, Bloomberg School of Public Health, 615 N. Wolfe Street, Room E-7616, Baltimore, MD 21205. E-mail: san@jhsph.edu

Am J Respir Cell Mol Biol Vol 35. pp 55–64, 2006
Originally Published in Press as DOI: 10.1165/rcmb.2005-0453OC on February 16, 2006
Internet address: www.atsjournals.org

Underlying dynamics of the CSK are not well defined, however. We focus here upon the CSK of the ASM cell isolated from the two highly inbred strains of rat: the relatively hyporesponsive Lewis rat versus the relatively hyperresponsive Fisher rat (17–22). We present evidence that the strain-related differences in the ability of the isolated ASM cell to stiffen, to contract, and to remodel its CSK are consistent with differences in AHR observed *in vivo*. Moreover, the cell from the more contractile phenotype (Fisher) is shown to possess a higher content of ATP and a higher effective temperature of its cytoskeletal lattice (23–26). These findings provide an integrative framework that helps to illuminate the biophysical properties of the ASM cell and their potential contributions to the pathophysiology of AHR in asthma.

MATERIALS AND METHODS

Materials and Reagents

Tissue culture reagents were obtained from Sigma (St. Louis, MO), with the exception of Dulbecco's modified Eagle's medium–Ham's F-12 (1:1), which was purchased from Gibco (Grand Island, NY). The synthetic Arg-Gly-Asp (RGD) peptide (Peptite 2000; Integra Life Sciences, San Diego, CA) was provided by Dr. Juerg Tschopp. The ENLITEN ATP Assay System Bioluminescence Detection Kit was purchased from Promega (Madison, WI). All other reagents and drugs were obtained from Sigma. Serotonin (5-hydroxytryptamine [5-HT]), bradykinin, acetylcholine, carbamylcholine chloride (carbachol), isoproterenol (ISO), and N^6,2′-O-dibutyryladenosine 3′,5′-cyclic monophosphate (db-cAMP) were reconstituted in sterile distilled water, frozen in aliquots, and diluted appropriately in serum-free media on the day of use.

Animals

The highly inbred Fisher 344 and Lewis rat strains (male, 7–9 wk old) were obtained from a commercial supplier (Harlan Sprague-Dawley, Inc., Indianapolis, IN) and housed in a conventional animal care facility at Harvard School of Public Health (Boston, MA). The animal protocols were approved by Harvard Medical Area Standing Committee on Animal Resources and Comparative Medicine and complied with Federal and State regulations governing the humane care and use of laboratory animals.

Cell Isolation and Culture

Rat tracheal ASM cells were prepared as previously described (10, 11), grown until confluence at 37°C in humidified air containing 5% CO_2, and passaged with 0.25% trypsin-0.02% EDTA solution every 10–14 d. In the present study, we used cells in passages 3–7 that were derived from five different animals for each strain (Lewis versus Fisher rats). Unless otherwise specified, serum-deprived cells were plated at 30,000 cells/cm^2 on plastic wells (96-well Removawell, Immulon II; VWR International, West Chester, PA) previously coated with type I collagen (Vitrogen 100; Cohesion, Palo Alto, CA) at 500 ng/cm^2. Cells were maintained in serum-free media for 24 h at 37°C in humidified air containing 5% CO_2. These conditions have been optimized for seeding cultured cells on collagen matrix and for assessing their mechanical properties (10, 11, 27, 28).

Optical Magnetic Twisting Cytometry

Stiffness of each individual ASM cell was measured as described previously (23). Briefly, an RGD-coated ferrimagnetic microbead bound to adherent cell was magnetized horizontally (parallel to the surface on which cells were plated) with a brief 1,000-Gauss pulse and twisted in a vertically aligned homogenous magnetic field (20 Gauss) that was varying sinusoidally in time; measurements were performed at a single frequency of 0.75 Hz or oscillatory frequencies between 10^{-1} and 10^{3} Hz. The sinusoidal twisting magnetic field caused a rotation and a pivoting displacement of the bead: As the bead moves, the cell develops internal stresses that resist bead motion (23). Lateral bead displacements in response to the resulting oscillatory torque were detected optically (in spatial resolution of $\sim$ 5 nm), and the ratio of specific torque to bead displacements was computed and expressed as the cell stiffness in units of Pascals (Pa) per nanometer.

For each individual ASM cell, stiffness was measured for the duration of 300 or 600 s; baseline stiffness was measured for the first 0–60 s, and changes in cell stiffness in response to various contractile agonists (serotonin, bradykinin, acetylcholine, and carbachol) and relaxing agonists (isoproterenol and db-cAMP) were measured continuously up to the indicated time (60–300 s or 60–600 s). For each cell, stiffness was normalized to its baseline stiffness before the agonist stimulation.

Fourier Transform Traction Microscopy

A detailed description of this technique is given by Butler and colleagues (29–31). Using traction microscopy, we measured the distribution of contractile stresses arising at the interface between each adherent cell and its substrate (traction field) and their change in response to increasing concentrations of 5-HT (0.1, 1, and 10 μM) or ISO (0.1, 1, and 10 μM). In brief, ASM cells were plated sparsely on a polyacrylamide elastic gel block coated with collagen Type I (0.2 mg/ml) and allowed to spread and stabilize for 6 h. Images of 0.2-μm diameter fluorescent microbeads (Molecular Probes, Eugene, OR) embedded near the gel apical surface were taken at different times (before and after a 5-min treatment with agonists). The fluorescent image of the same region of the gel after trypsin was used as the reference (traction-free) image. The displacement field between a pair of images was obtained by identifying the coordinates of the peak of the cross-correlation function (29–31).

From the displacement field and known elastic properties of the gel (Young's modulus of the gel was determined to be $\sim$ 8,000 Pa, and a Poisson's ratio was taken to be 0.48), the traction field was calculated using constrained and unconstrained Fourier transform traction cytometry (FTTC) as described previously (29–31). The computed traction field was used to obtain (*1*) the contractile stress (pre-stress), defined as the net tensile force transmitted by the actin CSK across a cross-sectional area of the cell per unit area and (*2*) the contractile moment, which is a scalar measure of the cell's contractile strength (29, 30). In this study, pre-stress is expressed in Pa, and contractile moment is expressed in pico-Newton meters (pNm).

Spontaneous Nanoscale Bead Motion

The remodeling dynamics of the CSK network was measured as described previously (11, 25). Under microscopic observation, we visualized spontaneous nanoscale movements of an individual RGD-coated microbead tightly anchored to the CSK of the ASM cell ($\sim$ 50–100 beads per field of view) and recorded its positions every 83 ms. The trajectories of bead motions in two dimensions were characterized by computing the mean square displacement of all beads as function of time [MSD(t)] (nm^2):

$$\text{MSD (t)} = \frac{1}{N}\sum_{i=1}^{N} r_i(t)^2 \qquad (1)$$

where $r_i(t)$ is the distance of the *i*th bead at time t relative to its position at t = 0. The MSD was computed at intervals that were equally spaced in time (1.3 s). Bead motions were corrected for the confounding effects of microscope stage drift; the stage drift was estimated from changes of the mean position of all beads within a field of view. The limit of resolution in our system was on the order of $\sim$ 10 nm, but by 10 s most beads had displaced a much greater distance. Accordingly, we analyzed MSD data for times greater than 10 s and up to 300 s. As shown in Results, the MSD of RGD-coated microbeads increased with time according to a power law relationship,

$$\text{MSD (t)} = D^*\,(t/t_o)^{\alpha}. \qquad (2)$$

The coefficient D* and the exponent α of the bead motion were estimated from a least-square fit of a power-law to the ensemble average of MSD data versus time; we take t_o to be 1 s and express D* in units of nm^2.

ATP Content

Cellular ATP concentrations were assayed with an ENLITEN ATP Assay System Bioluminescence Detection Kit (Promega) according to the manufacturer's directions. In brief, ATP was extracted with 2% trichloroacetic acid, and trichloroacetic acid in the sample was diluted to $< 0.1\%$ and neutralized to pH 7.75 with Tris-acetate. Based on the luciferase reaction, the emission of light (560 nm) was measured with a TD-20/20 luminometer (Turner BioSystems, Sunnyvale, CA). On each day of the experiments, sample relative luminescence unit (RLU) values were corrected for the background RLU (extractant/sample buffer) and converted to ATP mass from the ATP standard curve. In this study, ATP concentrations (nM) were normalized to the level of the total cell count.

Statistical Analysis

Unless otherwise noted, data are presented as means ± SE; *n* represents the number of cells. Statistical differences were determined by Student's *t* test for comparison of two sample means or ANOVA for comparison of more than two sample means followed by Bonferroni post-hoc testing for multiple comparisons between two sample means ($P < 0.05$ was considered statistically significant).

RESULTS

Stiffness

Under resting conditions, ASM cells isolated from the relatively hyporesponsive Lewis rat exhibited slightly higher baseline stiffness (1.11 ± 0.02 Pa/nm at 0.75 Hz) compared with cells isolated from the relatively hyperresponsive Fisher rat (0.78 ± 0.02 Pa/nm at 0.75 Hz). For both, cell stiffness increased in a time- and dose-dependent manner and reached a steady-state level within 5 min of stimulation with contractile agonist serotonin (5-HT). At each dose of 5-HT (0.1, 1, or 10 μM), cells isolated from the Fisher rat showed greater cell stiffening responses (Figure 1). In response to a panel of other contractile agonists that are known to increase intracellular Ca^{2+} concentration or inositol 1,4,5-trisphosphate formation via different receptor-mediated systems, Fisher ASM cells consistently demonstrated greater increases in stiffness (Figure 2).

When stimulated with progressively increasing doses of relaxing agonist ISO, two interesting observations were made (Figure 3). First, at the relatively lower doses of ISO (0.01 and 0.1 μM), cells isolated from Fisher and Lewis rat strains showed transient decreases in stiffness; cell stiffness decreased initially and then increased appreciably back toward the baseline stiffness. At these doses of ISO (0.01 and 0.1 μM), Fisher ASM cells were more resistant to the decrease in cell stiffness, however. Second, at the relatively higher doses of ISO (1 and 10 μM), cell stiffness of both strains of rat ASM decreased in a time- and dose-dependent manner and reached a steady-state level within 5 min; there were no statistical differences in the extent of the decrease between the two. For both rat strains, cell stiffness also decreased similar amounts in response to a cell-permeable cAMP analog, db-cAMP (Figure 4). Considering the ability of these cells to change stiffness from their most relaxed state to their most contracted state—corresponding to their contractile scope—that of cells isolated from the Fisher rat (4.4-fold) was substantially greater than that of the Lewis rat (3.4-fold).

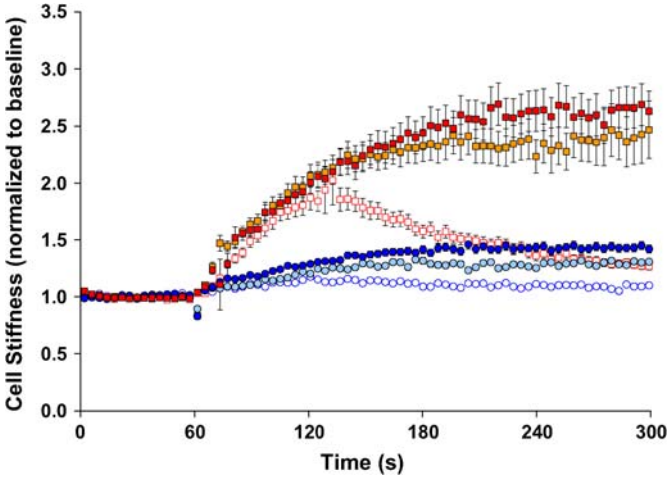

Figure 1. Stiffness changes in response to 5-HT. ASM cells isolated from the relatively hyporesponsive Lewis rat (*circles*) and the relatively hyperresponsive Fisher rat (*squares*) were stimulated with increasing doses of 5-HT (0.1 μM, *blue open circles*, *red open squares*; 1 μM, *teal closed circles*, *gold closed squares*; 10 μM, *blue closed circles*, *red closed squares*). For each cell, stiffness was measured continuously for 300 s. Baseline stiffness was measured for the first 0–60 s, and a change in stiffness in response to 5-HT was measured up to the indicated time (60–300 s). At each dose of 5-HT, changes in cell stiffness were normalized to the baseline stiffness of each individual cell before stimulation. Data are recorded at intervals that were equally spaced in time (1.3 s) but, for clarity, are suppressed and presented at intervals of 3.9 s. Data are presented as mean ± SE (n = 279–348 cells).

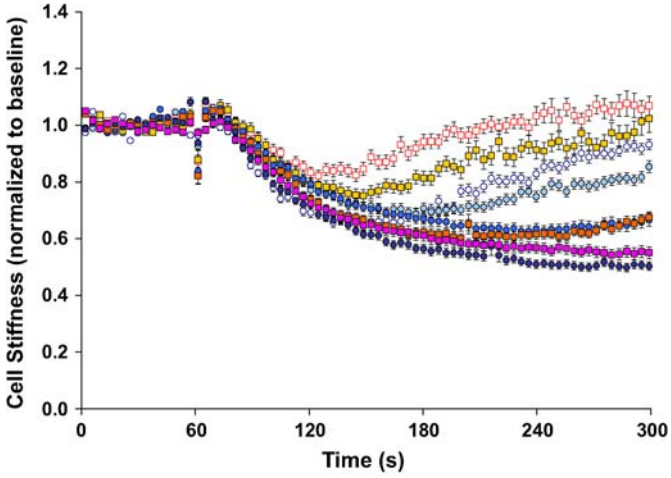

Figure 3. Stiffness changes in response to β-agonist. ASM cells isolated from the relatively hyporesponsive Lewis rat (*circles*) and the relatively hyperresponsive Fisher rat (*squares*) were stimulated with increasing doses of ISO (0.01 μM, *blue open circles*, *red open squares*; 0.1 μM, *teal closed circles*, *gold closed squares*; 1 μM, *blue closed circles*, *red closed squares*; 10 μM, *purple closed circles*, *pink closed squares*). At each dose of ISO, changes in cell stiffness were normalized to the baseline stiffness of each individual cell before stimulation. For clarity, data are presented at intervals of 3.9 s. Data are presented as mean ± SE (n = 197–346 cells).

Contractile Forces

Using traction microscopy, we quantified the level of contractile stresses generated by individual rat ASM cells (Lewis versus Fisher), their contractile moments, and their changes in response to contractile (5-HT) and relaxing (ISO) agonists. Figure 5 shows a phase-contrast image of a rat ASM cell cultured on a flexible polyacrylamide gel and the corresponding traction fields computed from the respective bead displacement fields using constrained FTTC. Arrows in Figure 5 show relative magnitudes and directions of the tractions, and colors show the magnitude of the traction vector. In general, the greatest tractions were at the cell periphery and directed centripetally.

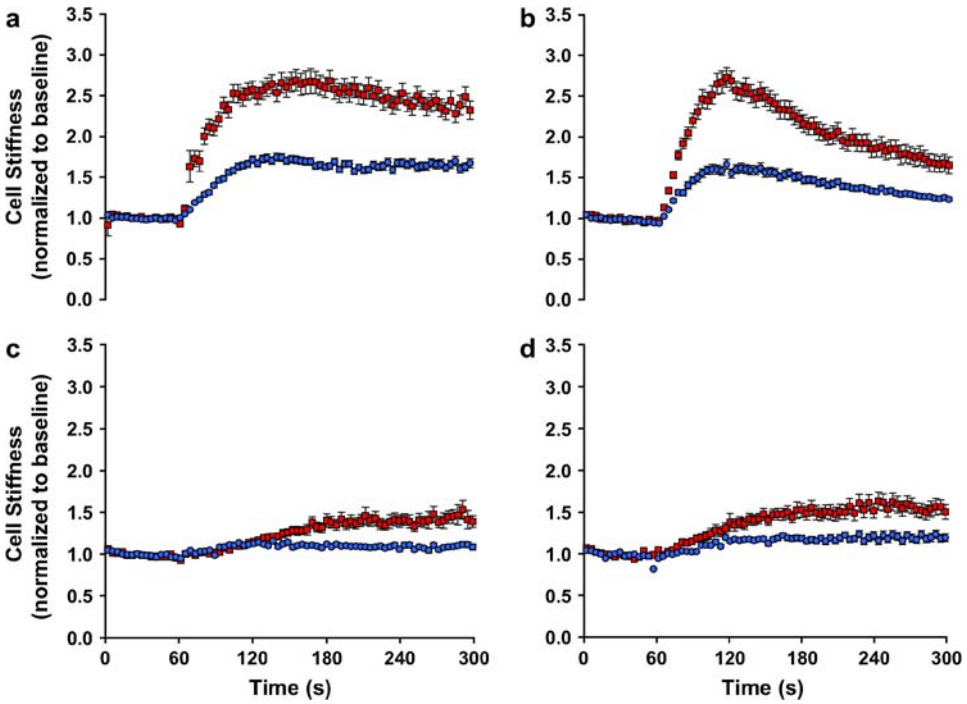

Figure 2. Stiffness changes in response to a panel of contractile agonists. ASM cells isolated from the relatively hyporesponsive Lewis rat (*blue closed circles*) and the relatively hyperresponsive Fisher rat (*red closed squares*) were maximally stimulated with a panel of contractile agonists: (*a*) 5-HT (1 μM); (*b*) bradykinin (1 μM); (*c*) acetylcholine (1 μM); (*D*) carbachol (100 μM). For each agonist, changes in cell stiffness were normalized to the baseline stiffness of each individual cell before stimulation. For clarity, data are presented at intervals of 3.9 s. Data are presented as mean ± SE (n = 473–804 cells).

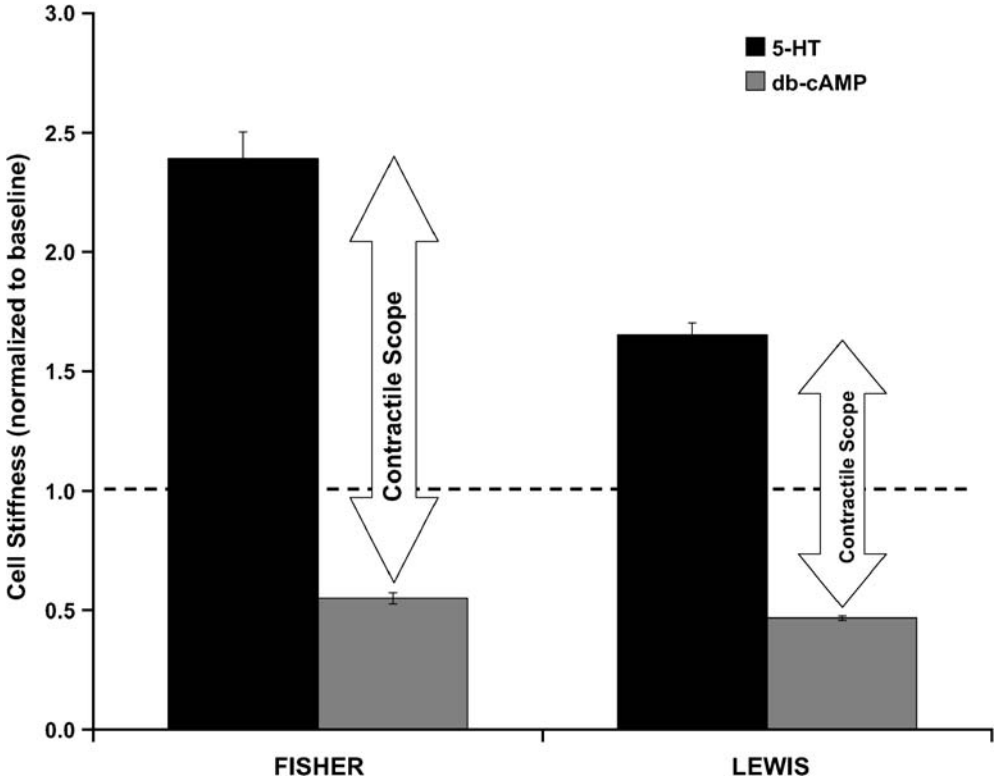

Figure 4. Stiffness changes in response to db-cAMP. ASM cells were stimulated for 600 s with a cell-permeable cAMP analog, db-cAMP (1 mM), and changes in cell stiffness were normalized to the baseline stiffness of each individual cell before stimulation. Data from Figure 2 (1 μM, 5-HT) are plotted to show the extent of the stiffening response (contractile scope). Data are presented as mean ± SE (n = 672–722 cells).

Under baseline conditions, compared with cells isolated from the Lewis rat (2,320 ± 260 Pa), cells isolated from the Fisher rat (3,221 ± 330 Pa) exerted greater contractile stress. Although computation of contractile stress is influenced by the estimation of cell size and shape (29, 30), the projected areas of these cells were not statistically different (Fisher 7,928 ± 563 μm^2 versus Lewis 6,744 ± 467 μm^2). Nonetheless, to avoid systematic errors that might be associated with the estimation of cell geometry, from the traction field (Figure 6), we computed the contractile moment, which is a measurement of contractile strength that requires no estimation of cell geometry. Compared with cells isolated from the relatively hyporesponsive Lewis rat

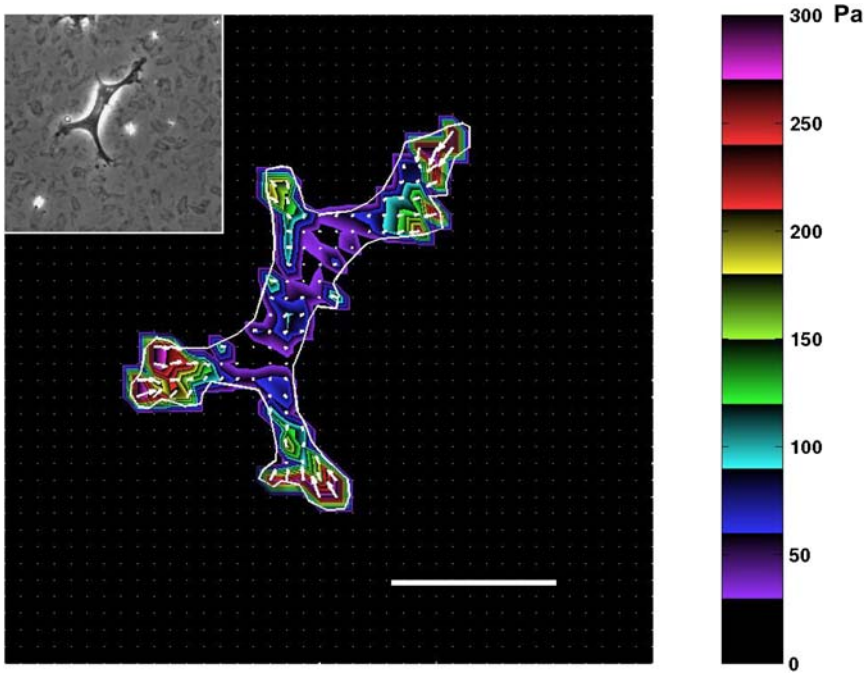

Figure 5. Traction field map of the ASM cell on the elastic substrate. Rat ASM cells were sparsely plated on the polyacrylamide gel coated with collagen type I. The traction field was computed from the displacement field using constrained FTTC; the cell boundary is shown by the *white line*. *Colors* show the magnitude of the tractions in Pa (*see* color scale). *Arrows* show the direction and relative magnitude of the tractions. Young's modulus of the gel was 8,000 Pa. *Inset*: A phase-contrast image of the ASM cell. Scale bar, 50 μm.

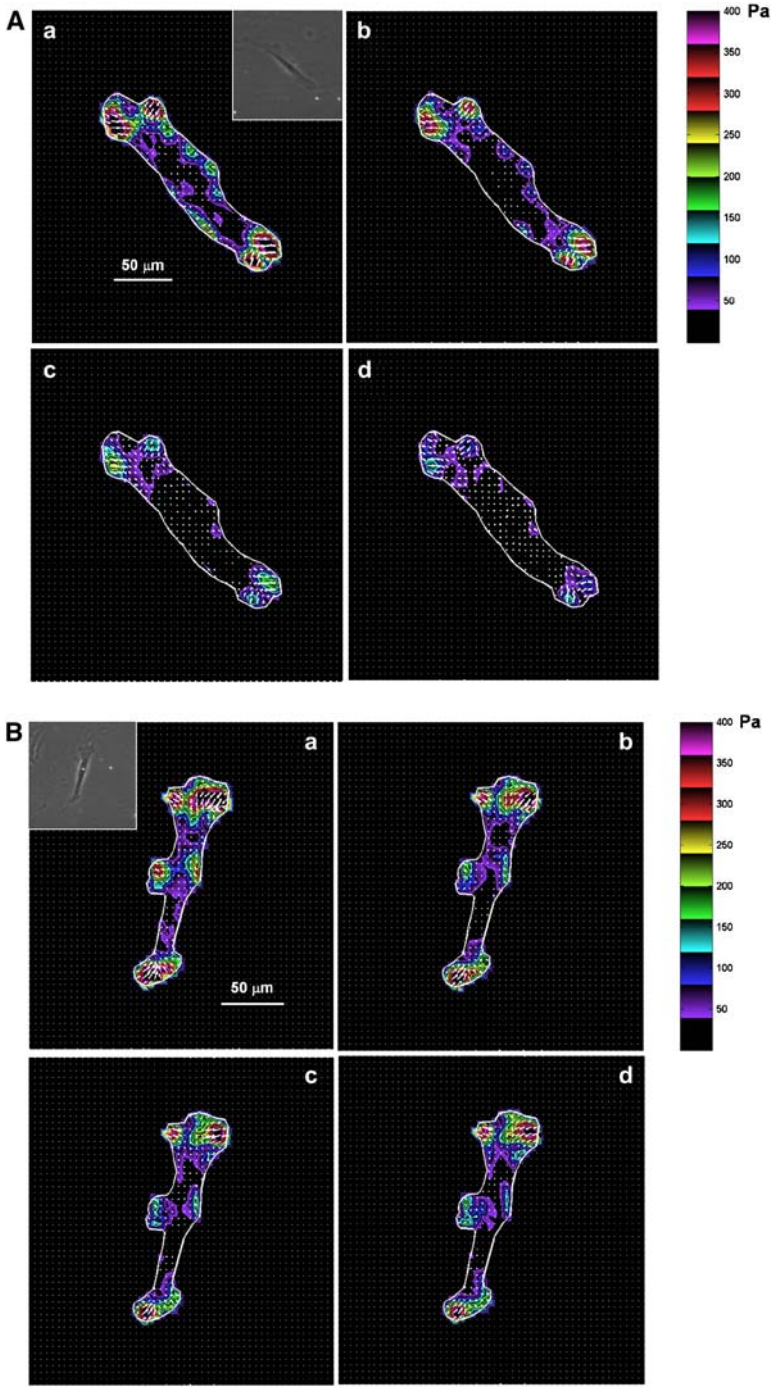

Figure 6. Traction field changes in response to β-agonist. (*A*) Representative changes in traction field of Fisher ASM cell. (*B*) Representative changes in traction field of Lewis ASM cell. Both cells were stimulated sequentially with increasing doses of ISO: (*a*) 0 μM; (*b*) 0.1 μM; (*c*) 1 μM; (*d*) 10 μM. *Colors* show the magnitude of the tractions in Pa (see color scale). *Arrows* show the direction and relative magnitude of the tractions.

(52.7 ± 10.2 pNm), cells isolated from the relatively hyperresponsive Fisher rat (81.4 ± 13.0 pNm) exhibited a significantly higher contractile moment.

When stimulated with progressively increasing doses of 5-HT (0.1, 1, and 10 μM), contractile moments increased for both strains of rat ASM cells; however, the increases were not statistically different from their respective baseline conditions (data not shown). These cells therefore exhibit basal tones that are close to their maximally contracted state. When stimulated with progressively increasing doses of ISO (0.1, 1, and 10 μM), contractile moments decreased for both strains of rat ASM cells (Figure 7). Compared with cells isolated from the relatively hyporesponsive Lewis rat, however, cells isolated from the relatively hyperresponsive Fisher rat exhibited greater extent of decrease in their contractile moments (Figure 7).

CSK Remodeling

To probe cytoskeletal remodeling dynamics, we measured spontaneous nano-scale movements of individual RGD-coated microbeads that were tightly anchored to the CSK (11, 25). Spontaneous motions of RGD-coated beads were characteristically different from motions of the beads coated with acetylated low-density lipoprotein, which bind to scavenger receptors thought to be floating in the cell membrane and exhibit simple Brownian motions (11). Acutely depleting cholesterol from the lipid membrane with methyl-β-cyclodextrin (32) increased membrane

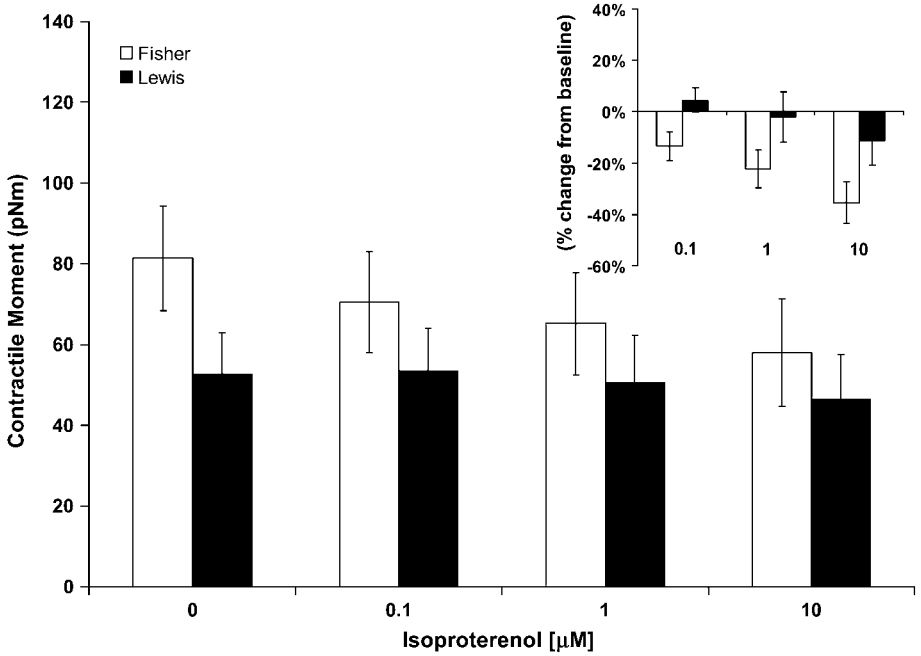

Figure 7. Contractile moment changes in response to β-agonist. ASM cells isolated from the relatively hyporesponsive Lewis rat and the relatively hyperresponsive Fisher rat were stimulated with increasing doses of ISO (0, 0.1, 1, and 10 μM). Contractile moment was calculated directly from the mean traction and expressed in units of pNm. No assumptions are made regarding the shape of the cell. *Open bars* represent Fisher ASM cells; *closed bars* represent Lewis ASM cells. *Inset*: For each cell, calculated contractile moment in response to ISO (0.1, 1, and 10 μM) is expressed as a percentage change from respective baseline. Data are presented as mean ± SE (n = 12 cells for each group).

stiffness as probed by optical magnetic twisting cytometry (OMTC) with acetylated low-density lipoprotein–coated beads and greatly reduced the spontaneous lateral mobility of those same beads (data not shown). However, cholesterol depletion had little effect on CSK stiffness and lateral mobility of RGD-coated beads (data not shown).

Over the course of 5 min, the trajectory of each RGD-coated bead (4.5 μm in diameter) anchored to the CSK of the ASM cell (Fisher and Lewis) displayed random motions that amounted to a small fraction of the bead diameter (~ 0.4 μm). For both, MSD was found to grow in an unbounded fashion with time and, more specifically, varied with time as a power law (Figure 8): MSD increased with time as $\sim t^{1.6}$, whereas an exponent of unity would be expected for a simple passive diffusion. These observations, taken together with our previous findings (11, 25), are inconsistent with simple Brownian motion. Instead, they are

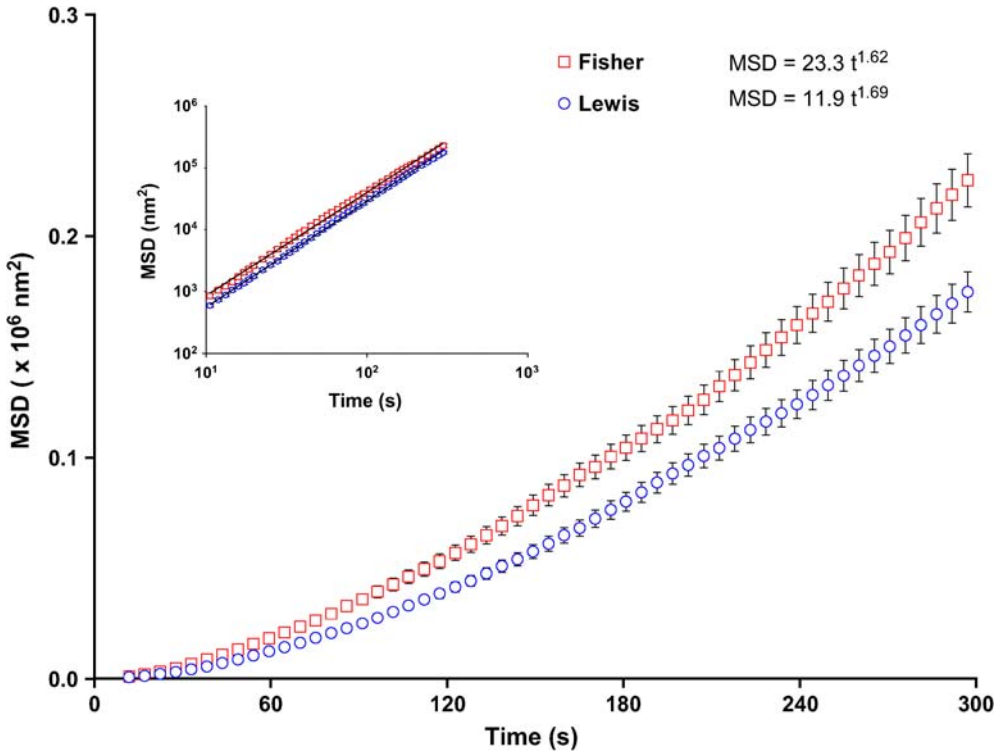

Figure 8. The rate of cytoskeletal remodeling in the ASM cell. Spontaneous bead motions are quantified by their MSD as function of time (Eq. 1). For both cells (Lewis, *blue open circles*; Fisher, *red open squares*), the MSD increases with time according to a power law relationship. *Inset*: The coefficient D* and the exponent α of the bead motion were estimated from a least squares fit of a power law to the MSD data versus time. The MSDs were computed at intervals that were equally spaced in time (1.3 s). For clarity, we have suppressed many of these data and left only data at approximately logarithmically spaced intervals. Data are presented as mean ± SE (n = 1,006–1,015 cells).

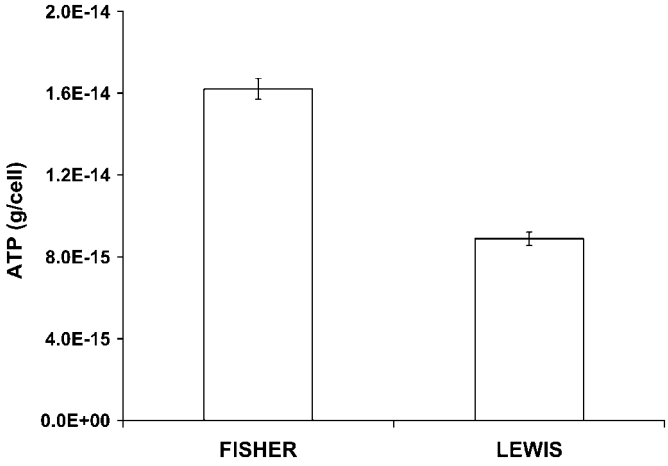

Figure 9. The content of ATP in the ASM cell. For both cells (Fisher versus Lewis), cellular ATP content was measured by the bioluminescence assay (Promega). On each day of the experiments, sample RLU values were corrected for the background RLU (extractant/sample buffer) and converted to ATP mass from the ATP standard curve. ATP concentrations (nM) were normalized to the level of the total cell count. Data are presented as mean ± SE (n = 6 wells).

consistent with the notion that these beads track motions of underlying structure to which they are attached and that such anomalous motions are superdiffusive.

Superdiffusive bead motions were appreciably different between cells isolated from the relatively hyporesponsive Lewis rat versus the relatively hyperresponsive Fisher rat (Figure 8). For the Fisher ASM cells, the coefficient D* (a measure of the extent of CSK remodeling) was bigger by a factor of 2 compared with Lewis ASM cells, and the superdiffusive exponent α was slightly smaller. We also observed similar relationships when these cells were adherent upon an elastic gel substrate that ranged from 1–20 kPa in stiffness, although differences in the coefficient D* between the two approached 5-fold at the lowest gel stiffness (data not shown). As such, compared with cells isolated from the relatively hyporesponsive Lewis rat, those isolated from the relatively hyperresponsive Fisher rat exhibited faster CSK remodeling (Figure 8). Consistent with the notion that these molecular-scale cytoskeletal rearrangements are ATP dependent (25), ASM cells isolated from the relatively hyperresponsive Fisher rat also exhibited higher intracellular ATP concentrations (Figure 9), suggesting higher metabolic or energy state of the cell.

Effective Temperature of the CSK

We have shown previously that the extent to which the ASM cell can regulate its mechanical properties and remodel its internal microstructures depends largely on its ability to modulate an effective temperature of its CSK matrix (23–26). To assess the extent to which this effective matrix temperature could help explain the observed biophysical properties, we measured the stiffness (g'), the loss modulus (g'') and loss tangent (η) over a wide frequency (f) range as described previously (23, 26).

Throughout the measurement range (oscillatory frequencies from 10^{-1} to 10^{3} Hz), the storage modulus g' of the ASM cell (Lewis and Fisher) increased with frequency as a weak power law (Figure 10). The loss modulus g'' also followed a weak power law at low frequencies (below $\sim$ 10 Hz) but showed stronger frequency dependence at higher frequencies (above $\sim$ 10 Hz). If g'(f) goes as $\sim f^{x-1}$, then the effective temperature is x (23, 26). The value of x varies between 1 and 2, with 1 corresponding to an elastic Hookean solid and 2 corresponding to a Newtonian viscous fluid. As such, x indicates where the material sits along a continuous spectrum of solid-like and liquid-like states (23, 24, 26).

Under resting conditions, the power-law frequency dependence of g' and g'' differed appreciably between the two rat strains (Lewis, $f^{0.17}$; Fisher, $f^{0.20}$) and thereby exhibited different levels of x (Figure 10). The effective temperature x can also be derived from the structural damping relationship $\eta = \tan[(x - 1)\pi/2]$, where η = g"/g' at 0.75 Hz (23, 33). Compared with cells isolated from the relatively hyporesponsive Lewis rat ($x = 1.164 \pm 0.001$; n = 1,288 cells), cells isolated from the relatively hyperresponsive Fisher rat ($x = 1.195 \pm 0.002$; n = 1,177 cells) exhibited significantly higher effective temperature ($P < 0.05$).

Consistent with data reported previously (23, 26), when these cells were activated by contractile agonist 5-HT, g' and g'' increased, and their dependence on frequency decreased (Figure 10). These changes were more prominent for Fisher ASM cells.

DISCUSSION

We have contrasted biophysical properties of the ASM cell isolated from the relatively hyporesponsive Lewis rat versus the relatively hyperresponsive Fisher rat. Compared with Lewis ASM cells, Fisher ASM cells showed similar decreases in stiffness in response to a panel of relaxing agonists (isoproterenol and db-cAMP) but demonstrated greater increases in stiffness in response to a panel of contractile agonists (serotonin, bradykinin, acetylcholine, and carbachol). Fisher ASM cells also exerted bigger contractile forces and exhibited greater scope of these forces. Finally, Fisher ASM cells showed faster CSK remodeling, which was consistent with higher intracellular ATP content and higher effective temperature of the CSK matrix (23–26). The ability of the ASM cell to modulate its mechanical properties and remodel its CSK was remarkably different between strains. These physical differences measured at the level of the single cell *in vitro* were consistent with strain-related differences in airway responsiveness *in vivo*.

Asthma and AHR

Asthma is a complex disease in which T helper-2–mediated inflammation interacts with structural changes to cause variable airflow obstruction (34, 35). AHR is a cardinal feature of asthma in which the airways narrow too easily and too much (1, 2). The link between the immunologic phenotype and the resulting mechanical phenotype associated with disease presentation, including AHR, remains poorly understood. It has been established that AHR can be uncoupled from airway inflammation (35–37). On the other hand, it remains unclear if AHR is due to structural and/or mechanical changes in the noncontractile elements of the airway wall (38), alterations in the coupling of the airway wall to the surrounding lung parenchyma (39, 40), or fundamental changes in the amount (41, 42), phenotype (4), or plasticity (remodeling) of the ASM cell (12–16). In the present study, we considered one such paradigm and focused upon physical features of the ASM cell—the key end-effector of acute airway narrowing—that could account for AHR.

As a model system, we used ASM cells in culture. Cells in culture have certain limitations but offer the advantages that ASM cells passaged in culture retain pharmacomechanical coupling to a wide panel of contractile and relaxing agonists (28, 43–47) and, with recent technological advances, can be characterized biophysically (10, 11, 23, 25, 29–31, 48, 49). This article establishes that comprehensive biophysical characterization of bronchospasm in culture is a reality, and these characterizations

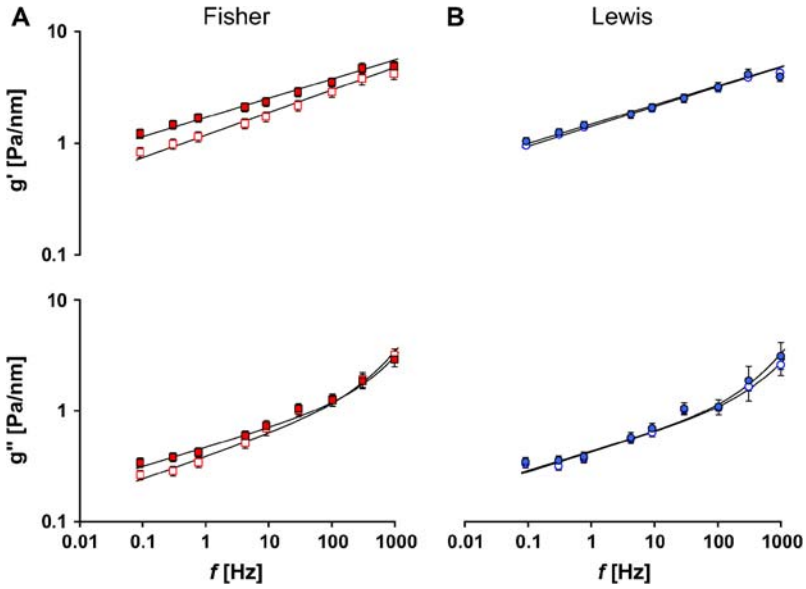

Figure 10. Stiffness g′ (*top*) and loss modulus g″ (*bottom*) versus frequency. The *solid lines* are the fit of experimental data to the structural damping equation with addition of a Newtonian viscous term as previously described (23). Fitting was performed by nonlinear regression analysis. *Blue open circles* represent baseline g′ and g″, and *blue closed circles* represent g′ and g″ of Lewis ASM cells in response to 1 μM 5-HT. *Red open squares* represent baseline g′ and g″, and *red closed squares* represent g′ and g″ of Fisher ASM cells in response to 1 μM 5-HT. Data are presented as mean ± SE (n = 43–62 cells).

indicate mechanical responsiveness that is consistent with physiologic responses measured at tissue and organ levels (50, 51).

AHR and ASM

Fisher rats have more ASM in their airways (18) and show greater capacity to proliferate in cell culture (52); these features are analogous to that found in ASM cells from humans with asthma (7, 42, 43, 53, 54). Although the source of the increased cell number (increased proliferation, decreased apoptosis, and/or increased migration) remains to be elucidated (52, 53, 55–57), increased muscle quantity (mass) and increased muscle quality (contractility) would be expected to predispose toward AHR (18, 39, 40, 58). However, it remains unclear if muscle mass and contractility might covary. For example, it is likely that the ASM cell in the proliferative/synthetic/maturational state might be less contractile than similar cells differentiated into fully contractile state—an effect that would be compensatory—but no mechanical data are available to support that possibility. In this article we deal only with the issue of contractility of ASM cells rather than their number and demonstrate appreciable differences in responses between strains.

Stiffness

At the level of the single cell *in vitro*, we showed that the ASM cell isolated from the relatively hyperresponsive Fisher rat exhibited greater stiffening responses compared with cells isolated from the relatively hyporesponsive Lewis rat (Figures 1–4). Fisher ASM cells, when activated by 5-HT, also stiffen fast and stiffen more (Figures 1, 2, and 10). These physical responses were not limited to one agonist but were common for a panel of contractile agonists that are known to increase Ca^{2+} concentration or inositol 1,4,5-trisphosphate formation (Figure 2).

The ranked order of these agonists in this study was characteristically different from those reported in isolated tracheal segments and in intact rats; in tissues and intact animals, the muscarinic cholinergic receptor agonists cause greater constrictor responses than 5-HT or bradykinin (17–22, 46, 47, 59). Here we found that 5-HT and bradykinin caused greater stiffening responses in the isolated ASM cells. We do not know why the isolated cells in culture were less responsive to the muscarinic cholinergic receptor agonists; we speculate a lower expression of these receptors. In rat ASM cells, 5-HT and bradykinin lead to increases in intracellular Ca^{2+} and, in particular, the Fisher ASM cells exhibit greater increases compared with the Lewis ASM cells (46, 47, 59). Our findings are in agreement with these biochemical findings in these cells, and we now provide direct mechanical evidence that cells from the more contractile phenotype (Fisher rat) demonstrate greater increases in stiffness.

Tidal muscle stretches caused by deep inspirations are the most potent of all known bronchodilatory agencies (60), but the stiffer the muscle is the less it stretches in response to tidal breathing and deep inspirations (5, 24, 61). There is a positive feedback, therefore, in which stretch keeps the muscle compliant, thus facilitating further stretch and keeping the muscle dynamically equilibrated, compliant, and long (16, 61–64). Conversely, if the muscle stretches less, it gets stiffer, and if it gets stiffer the system stretches less still. In that eventuality, Fredberg and colleagues (60, 65, 66) have proposed that actin–myosin bonds become stuck or "frozen" in the latch state (67) and that the muscle can become refractory to the bronchodilating effects of a deep inspiration. Although in this study we considered only isometric contractions, cells isolated from Fisher rats also show an attenuated decrease in stiffness in response to the relatively lower doses of relaxing agonist ISO (Figure 3). These findings, taken together with the findings of earlier reports (17–22, 68), suggest that the dynamics of actin–myosin interactions and therefore contractility of the ASM cell may be fundamentally different between the two highly inbred strains of rat.

Contraction, Rate Processes, and Remodeling Dynamics

For the reasons described previously, ASM stiffness is innately important. Stiffness and its changes are also indirect indices of contractility (10, 28, 61), but in this study we also used traction microscopy to obtain direct measures of cell contractility (29–31).

Although a potential link between altered ASM contractility and AHR in asthma remains to be established, studies have reported differences in muscle shortening velocity in cases of allergen-sensitized animal models (69–71), an array of highly inbred strains of rodents (68, 72), and normal human bronchi passively sensitized with human serum from atopic individuals (73). More recently, Ma and colleagues (7) have shown that bronchial ASM cells isolated from subjects with asthma shorten faster and shorten more than normal cells do. Here we provide evidence that ASM cells isolated from the relatively hyperresponsive

Fisher rat not only stiffen more and exert bigger contractile forces, but also stiffen faster and demonstrate greater contractile scope.

Contraction of the ASM cell is driven by the myosin motor, and myosin exerts its mechanical effects within an integrated cytoskeletal scaffolding that is in a continuous state of remodeling (8–11, 14). This remodeling is thought to be a major factor contributing to excessive airway narrowing in asthma (12–16), but the extent of this remodeling and its rate of progression are not well defined.

In our previous studies (11, 25), we described a novel assay that probes the rate of molecular-scale events in the living cell. This assay is based on spontaneous nanoscale motions of microbeads coated with a peptide containing Arg-Gly-Asp (RGD). Such beads bind to cell surface integrin receptors (27) and form focal adhesions (74); they become well integrated into the CSK scaffold (10, 27) and display tight functional coupling to stress-bearing cytoskeletal structures and the contractile apparatus (10, 30, 48). Unlike Brownian motions that are driven passively by thermal forces, spontaneous motions of RGD-coated beads show anomalous, superdiffusive motions that are in keeping with the concept that they track active, ongoing rearrangements (remodeling) of underlying structures to which they are firmly attached (11, 25).

Here we have shown that the rate of such remodeling is appreciably different between strains. Compared with cells isolated from the relatively hyporesponsive Lewis rat, cells isolated from the relatively hyperresponsive Fisher rat demonstrated a greater rate of remodeling. Fisher ASM cells also exhibited higher intracellular ATP content and a higher effective temperature of the CSK matrix. As described elsewhere (23–26), these observations seem to fit within the framework of molecular trapping in deep energy wells and molecular hopping out of those wells driven by an effective matrix temperature.

Conclusion

We have reported over a wide range of cell types, probing technologies, molecular couplings, time scales, and manipulations that when the mechanical properties of the cell change, they do so along a special trajectory that is controlled by an effective matrix temperature (23, 25, 26). The effective temperature indicates where a particular cell sits on the spectrum between solid-like and liquid-like states (23, 24). Here we show that the more contractile Fisher ASM cells exhibit a greater rate of remodeling and have higher effective temperature of the CSK matrix. These observations suggest that Fisher ASM cells are in a relatively "hotter" (i.e., liquid-like) state, whereas Lewis ASM cells are in relatively "colder" (i.e., solid-like) state (23, 24). The "hotter" Fisher ASM cells are more conducive to remodel their internal microstructures. We also demonstrate that upon contractile activation, Fisher ASM cells quickly modulate effective matrix temperature (i.e., become "colder"), which favors these cells to stiffen fast and stiffen more and to generate bigger contractile forces. We offer an integrative framework by which an effective temperature of the CSK matrix could illuminate upon biophysical properties of the ASM cell—the ability of the CSK to deform, to flow, and to remodel—and their potential contributions to AHR. Moreover, these physical attributes may explain, and even scale-up to, phenotypic differences in airway responsiveness *in vivo*.

Conflict of Interest Statement: None of the authors has a financial relationship with a commercial entity that has an interest in the subject of this manuscript.

Acknowledgments: The authors thank Dr. James G. Martin (Meakins-Christie Laboratories, McGill University) for critical reading of this manuscript and for helpful insights and Ms. Elizabeta Gorgoska (Harvard School of Public Health) for technical assistance.

References

1. Woolcock AJ, Peat JK. Epidemiology of bronchial hyperresponsiveness. *Clin Rev Allergy* 1989;7:245–256.
2. Sterk PJ, Bel EH. Bronchial hyperresponsiveness: the need to distinguish between hypersensitivity and excessive airway narrowing. *Eur Respir J* 1989;2:267–274.
3. Black JL, Johnson PR. Airway smooth muscle in asthma. *Respirology* 1996;1:153–158.
4. King GG, Pare PD, Seow CY. The mechanics of exaggerated airway narrowing in asthma: the role of smooth muscle. *Respir Physiol* 1999; 118:1–13.
5. Fredberg JJ. Bronchospasm and its biophysical basis in airway smooth muscle. *Respir Res* 2004;5:2.
6. Solway J, Fredberg JJ. Perhaps airway smooth muscle dysfunction contributes to asthmatic bronchial hyperresponsiveness after all. *Am J Respir Cell Mol Biol* 1997;17:144–146.
7. Ma X, Cheng Z, Kong H, Wang Y, Unruth H, Stephens NL, Laviolette M. Changes in biophysical and biochemical properties of single bronchial smooth muscle cells from asthmatic subjects. *Am J Physiol* 2002;283: L1181–L1189.
8. Mehta D, Gunst SJ. Actin polymerization stimulated by contractile activation regulates force development in canine tracheal smooth muscle. *J Physiol* 1999;519:829–840.
9. Kuo KH, Wang L, Pare PD, Ford LE, Seow CY. Myosin thick filament lability induced by mechanical strain in airway smooth muscle. *J Appl Physiol* 2001;90:1811–1816.
10. An SS, Laudadio RE, Lai J, Rogers RA, Fredberg JJ. Stiffness changes in cultured airway smooth muscle cells. *Am J Physiol* 2002;283:C792–C801.
11. An SS, Fabry B, Mellema M, Bursac P, Gerthoffer WT, Kayyali US, Gaestel M, Shore SA, Fredberg JJ. Role of heat shock protein 27 in cytoskeletal remodeling of the airway smooth muscle cell. *J Appl Physiol* 2004;96:1707–1713.
12. Pratusevich VR, Seow CY, Ford LE. Plasticity in canine airway smooth muscle. *J Gen Physiol* 1995;105:73–94.
13. Gunst SJ, Meiss RA, Wu MF, Rowe M. Mechanisms for the mechanical plasticity of tracheal smooth muscle. *Am J Physiol* 1995;268:C1267–C1276.
14. Seow CY, Pratusevich VR, Ford LE. Series-to-parallel transition in the filament lattice of airway smooth muscle. *J Appl Physiol* 2000;89:869–876.
15. Wang L, Pare PD, Seow CY. Effect of chronic passive length change on airway smooth muscle length-tension relationship. *J Appl Physiol* 2001;90:734–740.
16. Gunst SJ, Wu MF. Plasticity of airway smooth muscle stiffness and extensibility: role of length-adaptive mechanisms. *J Appl Physiol* 2001;90: 741–749.
17. Martin JG, Bellofiore S, Guttmann RD. Strain-related differences in airway reactivity amongst highly inbred rats. *Am Rev Respir Dis* 1987;135:A473.
18. Eidelman DH, Dimaria GU, Bellofiore S, Wang NS, Guttmann RD, Martin JG. Strain-related differences in airway smooth muscle and airway responsiveness in the rat. *Am Rev Respir Dis* 1991;144:792–796.
19. Dandurand RJ, Xu LJ, Martin JG, Eidelman DH. Airway-parenchymal interdependence and bronchial responsiveness in two highly inbred rat strains. *J Appl Physiol* 1993;74:538–544.
20. Dandurand RJ, Wang CG, Phillips NC, Eidelman DH. Responsiveness of individual airways to methacholine in adult rat lung explants. *J Appl Physiol* 1993;75:364–372.
21. Jia Y, Xu L, Heisler S, Martin JG. Airways of a hyperresponsive rat strain show decreased relaxant response to sodium nitroprusside. *Am J Physiol* 1995;269:L85–L91.
22. Wang CG, Almirall JJ, Dolman CS, Dandurand RJ, Eidelman DH. In vitro bronchial responsiveness in two highly inbred rat strains. *J Appl Physiol* 1997;82:1445–1452.
23. Fabry B, Maksym GN, Butler JP, Glogauer M, Navajas D, Fredberg JJ. Scaling the mircrorheology of living cells. *Phys Rev Lett* 2001;87: 148102.
24. Gunst SJ, Fredberg JJ. The first three minutes: smooth muscle contraction, cytoskeletal events, and soft glasses. *J Appl Physiol* 2003;95:413–425.
25. Bursac P, Lenormand G, Fabry B, Oliver M, Weitz DA, Viasnoff V, Butler JP, Fredberg JJ. Cytoskeletal remodelling and slow dynamics in the living cell. *Nat Mater* 2005;4:557–561.

26. Laudadio RE, Millet EJ, Fabry B, An SS, Butler JP, Fredberg JJ. The rat airway smooth muscle cell during actin modulation: rheology and glassy dynamics. *Am J Physiol* 2005;289:C1388–C1395.
27. Wang N, Butler JP, Ingber DE. Mechanotransduction across the cell surface and through the cytoskeleton. *Science* 1993;260:1124–1127.
28. Hubmayr RD, Shore SA, Fredberg JJ, Planus E, Panettieri RA, Moller W, Heyder J, Wang N. Pharmacological activation changes stiffness of cultured human airway smooth muscle cells. *Am J Physiol* 1996; 271:C1660–C1668.
29. Butler JP, Tolic-Norrelykke IM, Fabry B, Fredberg JJ. Traction fields, moments, and strain energy that cells exert on their surroundings. *Am J Physiol* 2002;282:C595–C605.
30. Wang N, Tolic-Norrelykke IM, Chen J, Mijailovich SM, Butler JP, Fredberg JJ, Stamenovic D. Cell prestress. I: stiffness and prestress are closely associated in adherent contractile cells. *Am J Physiol* 2002;282: C606–C616.
31. Tolic-Norrelykke IM, Butler JP, Chen J, Wang N. Spatial and temporal traction response in human airway smooth muscle cells. *Am J Physiol* 2002;283:C1254–C1266.
32. Klein U, Gimpl G, Fahrenholz F. Alteration of the myometrial plasma membrane cholesterol content with β-cyclodextrin modulates the binding affinity of the oxytocin receptor. *Biochemistry* 1995;34:13784–13793.
33. Fredberg JJ, Stamenovic D. On the imperfect elasticity of lung tissue. *J Appl Physiol* 1989;67:2408–2419.
34. Vignola AM, Mirabella F, Costanzo G, Di Giorgi R, Gjomarkaj M, Bellia V, Bonsignore G. Airway remodeling in asthma. *Chest* 2003;123:417S–422S.
35. Holgate ST, Holloway J, Wilson S, Bucchieri F, Puddicombe S, Davies DE. Epithelial-mesenchymal communication in the pathogenesis of chronic asthma. *Proc Am Thorac Soc* 2004;1:93–98.
36. Crimi E, Spanevello A, Neri M, Ind PW, Rossi GA, Brusasco V. Dissociation between airway inflammation and airway hyperresponsiveness in allergic asthma. *Am J Respir Crit Care Med* 1998;157:4–9.
37. Holloway JW, Beghe B, Holgate ST. The genetic basis of atopic asthma. *Clin Exp Allergy* 1999;29:1023–1032.
38. Milanese M, Crimi E, Scordamaglia A, Riccio A, Pellegrino R, Walter Canonica G, Brusasco V. On the functional consequences of bronchial basement membrane thickening. *J Appl Physiol* 2001;91:1035–1040.
39. James AL, Pare PD, Hogg JC. The mechanics of airway narrowing in asthma. *Am Rev Respir Dis* 1989;139:242–246.
40. Macklem PT. A theoretical analysis of the effect of airway smooth muscle load on airway narrowing. *Am J Respir Crit Care Med* 1996;153:83–89.
41. Ebina M, Takahashi T, Chiba T, Motomiya M. Cellular hypertrophy and hyperplasia of airway smooth muscles underlying bronchial asthma: a 3-D morphometric study. *Am Rev Respir Dis* 1993;148:720–726.
42. Carroll N, Carello S, Cooke C, James A. Airway structure and inflammatory cells in fatal attacks of asthma. *Eur Respir J* 1996;9:709–715.
43. Panettieri RA, Murray RK, DePalo LR, Yadvish PA, Kotlikoff MI. A human airway smooth muscle cell line that retains physiological responsiveness. *Am J Physiol* 1989;256:C329–C335.
44. Ma X, Wang Y, Stephens NL. Serum deprivation induces a unique hypercontractile phenotype of cultured smooth muscle cells. *Am J Physiol* 1998;274:C1206–C1214.
45. Halayko AJ, Camoretti-Mercado B, Forsythe SM, Vieira JE, Mitchell RW, Wylam ME, Hershenson MB, Solway J. Divergent differentiation paths in airway smooth muscle culture: induction of functionally contractile myocytes. *Am J Physiol* 1999;276:L197–L206.
46. Tao FC, Tolloczko B, Eidelman DH, Martin JG. Enhanced Ca^{2+} mobilization in airway smooth muscle contributes to airway hyperresponsiveness in an inbred strain of rat. *Am J Respir Crit Care Med* 1999;160: 446–453.
47. Tao FC, Shah S, Pradhan AA, Tolloczko B, Martin JG. Enhanced calcium signaling to bradykinin in airway smooth muscle from hyperresponsive inbred rats. *Am J Physiol* 2003;284:L90–L99.
48. Hu S, Chen J, Fabry B, Numaguchi Y, Gouldstone A, Ingber DE, Fredberg JJ, Butler JP, Wang N. Intracellular stress tomography reveals stress focusing and structural anisotropy in the cytoskeleton of living cells. *Am J Physiol* 2003;285:C1082–C1090.
49. Smith BA, Tolloczko B, Martin JG, Grutter P. Probing the viscoelastic behavior of cultured airway smooth muscle cells with atomic force microscopy: stiffening induced by contractile agonist. *Biophys J* 2005; 88:2994–3007.
50. Fredberg JJ, Jones KA, Nathan M, Raboudi S, Prakash YS, Shore SA, Butler JP, Sieck GC. Friction in airway smooth muscle: mechanism, latch and implications in asthma. *J Appl Physiol* 1996;81:2703–2712.
51. Chitano P, Wang J, Cox CM, Stephens NL, Murphy TM. Different ontogeny of rate of force generation and shortening velocity in guinea pig trachealis. *J Appl Physiol* 2000;88:1338–1345.
52. Zacour ME, Martin JG. Enhanced growth response of airway smooth muscle in inbred rats with airway hyperresponsiveness. *Am J Respir Cell Mol Biol* 1996;15:590–599.
53. Johnson PR, Roth M, Tamm M, Hughes M, Ge Q, King G, Burgess JK, Black JL. Airway smooth muscle cell proliferation is increased in asthma. *Am J Respir Crit Care Med* 2001;164:474–477.
54. Roth M, Johnson PRA, Borger P, Bihl MP, Rudiger JJ, King GG, Ge Q, Hostettler K, Burgess JK, Black JL, *et al.* Dysfunctional interaction of C/EBPa and the glucocorticoid receptor in asthmatic bronchial smooth muscle cells. *N Engl J Med* 2004;351:560–574.
55. Madison JM. Migration of airway smooth muscle cells. *Am J Respir Cell Mol Biol* 2003;29:8–11.
56. Hirst SJ, Martin JG, Bonacci JV, Chan V, Fixman ED, Hamid QA, Herszberg B, Lavoie JP, McVicker CG, Moir LM, *et al.* Proliferative aspects of airway smooth muscle. *J Allergy Clin Immunol* 2004;114:S2–S17.
57. Lazaar AL, Panettieri RA. Airway smooth muscle: a modulator of airway remodeling in asthma. *J Allergy Clin Immunol* 2005;116:488–495.
58. Lambert RK, Wiggs BR, Kuwano K, Hogg JC, Pare PD. Functional significance of increased airway smooth muscle in asthma and COPD. *J Appl Physiol* 1993;74:2771–2781.
59. Tolloczko B, Jia YL, Martin JG. Serotonin-evoked calcium transients in airway smooth muscle cells. *Am J Physiol* 1995;269:L234–L240.
60. Gump A, Haughney L, Fredberg JJ. Relaxation of activated smooth muscle: relative potency of isoproterenol vs. tidal stretch. *J Appl Physiol* 2001;90:2306–2310.
61. Fredberg JJ, Inouye D, Miller B, Nathan M, Jafari S, Raboudi SH, Butler JP, Shore SA. Airway smooth muscle, tidal stretches, and dynamically determined contractile states. *Am J Respir Crit Care Med* 1997;156: 1752–1759.
62. Shen X, Wu MF, Tepper RS, Gunst SJ. Mechanisms for the mechanical response of airway smooth muscle to length oscillation. *J Appl Physiol* 1997;83:731–738.
63. Latourelle J, Fabry B, Fredberg JJ. Dynamic equilibration of airway smooth muscle contraction during physiological loading. *J Appl Physiol* 2002;92:771–779.
64. Dowell ML, Lakser OJ, Gerthoffer WT, Fredberg JJ, Stelmack GL, Halayko AJ, Solway J, Mitchell RW. Latrunculin B increases force fluctuation-induced relengthening of Ach-contracted, isotonically shortened canine tracheal smooth muscle. *J Appl Physiol* 2005;98: 489–497.
65. Fredberg JJ, Inouye DS, Mijailovich M, Butler JP. Perturbed equilibrium of myosin binding in airway smooth muscle and its implications in bronchospasm. *Am J Respir Crit Care Med* 1999;159:959–967.
66. Fredberg JJ. Frozen objects: small airways, big breaths, and asthma. *J Allergy Clin Immunol* 2000;106:615–624.
67. Hai CM, Murphy RA. Cross-bridge phosphorylation and regulation of latch state in smooth muscle. *Am J Physiol* 1988;254:C99–C106.
68. Blanc FX, Coirault C, Salmeron S, Chemla D, Lecarpentier Y. Mechanics and crossbridge kinetics of tracheal smooth muscle in two inbred rat strains. *Eur Respir J* 2003;22:227–234.
69. Antonissen LA, Mitchell RW, Kroeger EA, Kepron W, Tse KS, Stephens NL. Mechanical alterations of airway smooth muscle in a canine asthmatic model. *J Appl Physiol* 1979;46:681–687.
70. Jiang H, Rao K, Halayko AJ, Kepron W, Stephens NL. Bronchial smooth muscle mechanics of a canine model of allergic airway hyperresponsiveness. *J Appl Physiol* 1992;72:39–45.
71. Fan T, Yang M, Halayko A, Mohapatra SS, Stephens NL. Airway responsiveness in two inbred strains of mouse disparate in IgE and IL-4 production. *Am J Respir Cell Mol Biol* 1997;17:156–163.
72. Duguet A, Biyah K, Minshall E, Gomes R, Wang CG, Taoudi-Benchekroun M, Bates JHT, Eidelman DH. Bronchial responsiveness among inbred mouse strains. *Am J Respir Crit Care Med* 2000;161:839–848.
73. Mitchell RW, Ruhlmann E, Magnussen H, Leff AR, Rabe KF. Passive sensitization of human bronchi augments smooth muscle shortening velocity and capacity. *Am J Physiol* 1994;267:L218–L222.
74. Matthews BD, Overby DR, Alenghat FJ, Karavitis J, Numaguchi Y, Allen PG, Ingber DE. Mechanical properties of individual focal adhesions probed with a magnetic microneedle. *Biochem Biophys Res Commun* 2004;313:758–764.